

## On the Influence of State Selection on Mass Conservation in Dynamic Vapor Compression Cycle Models

Laughman, C.R.; Qiao, H.  
TR2016-151 December 2016

### Abstract

Many dynamic models of vapor compression systems experience nonphysical variations in the total refrigerant mass contained in the system when common modeling approaches are used. Rather than use the traditional state variables of pressure and specific enthalpy, the use of density as a state variable can eliminate these variations. The reasons for these variations are explained, and a set of test models is developed to study the effect of the state variable selection on the overall system charge. Results from both a simplified cycle model and a realistic air-source heat pump model indicate that this alternative approach has significant benefits for maintaining a fixed mass of refrigerant in the cycle.

*Mathematical and Computer Modeling of Dynamical Systems*

This work may not be copied or reproduced in whole or in part for any commercial purpose. Permission to copy in whole or in part without payment of fee is granted for nonprofit educational and research purposes provided that all such whole or partial copies include the following: a notice that such copying is by permission of Mitsubishi Electric Research Laboratories, Inc.; an acknowledgment of the authors and individual contributions to the work; and all applicable portions of the copyright notice. Copying, reproduction, or republishing for any other purpose shall require a license with payment of fee to Mitsubishi Electric Research Laboratories, Inc. All rights reserved.



Submitted to *Mathematical and Computer Modelling of Dynamical Systems*  
Vol. 00, No. 00, Month 20XX, 1–26

## On the Influence of State Selection on Mass Conservation in Dynamic Vapor Compression Cycle Models

Christopher R. Laughman<sup>†</sup> and Hongtao Qiao

*Mitsubishi Electric Research Laboratories, 201 Broadway, Cambridge, MA, USA*

*(Received 00 Month 20XX; final version received 00 Month 20XX)*

Many dynamic models of vapor compression systems experience nonphysical variations in the total refrigerant mass contained in the system when common modeling approaches are used. Rather than use the traditional state variables of pressure and specific enthalpy, the use of density as a state variable can eliminate these variations. The reasons for these variations are explained, and a set of test models is developed to study the effect of the state variable selection on the overall system charge. Results from both a simplified cycle model and a realistic air-source heat pump model indicate that this alternative approach has significant benefits for maintaining a fixed mass of refrigerant in the cycle.

**Keywords:** vapor compression cycle, fluid properties, simulation, mass conservation, Modelica

**AMS Subject Classification:** 80A10, 80M12

### 1. Introduction

Trends toward increased integration in building and transportation systems, as well as perennial demands for improved system performance, have continued to encourage interest in the development of dynamic models of vapor compression cycles. Such dynamic cycle models can be used for a variety of purposes, including system design, specification, control, and fault diagnostics, and can be applied to a wide variety of residential, commercial and industrial applications to understand and predict the behavior of field-installed systems. These dynamic models can also be coupled with models of other systems to examine and design the behavior of systems-of-systems to achieve specified requirements for the overall system and satisfy constraints that must be enforced on the physical hardware.

This wealth of interest in dynamic models of vapor compression cycles has resulted in a corresponding growth in both the literature and the number of documented models for these cycles [17]. The Modelica language [18] is particularly appropriate for the development of these system models, due to its object-oriented acausal modeling approach. This can be seen in the variety of references that have been published over the past 15 years regarding models of vapor compression cycles, such as those found in [16], among many others.

---

<sup>†</sup>Corresponding author. Email: laughman@merl.com

The performance of physical system models is often evaluated by comparing particular characteristics or outputs of their simulations to the related characteristics of an experimentally observed system. Since, as George E.P. Box said, “all models are wrong, but some are useful” [5], model creators and users must examine the most salient characteristics of their model to ensure that it accurately describes the behavior of interest. This is particularly important for complex physical systems such as vapor compression cycles; it is essential that engineers compare and validate dynamic cycle models against known experimental behavior and data before the model output can be expected to be reliable. One such variable that can easily be compared between simulation and experiment is the cycle’s refrigerant mass inventory, or charge, which is usually known to a fairly high degree of precision and is constant over extended time intervals. Such stability and ease of measurement is theoretically well-suited to use in model parameterization and calibration, and is convenient for study in dynamic system models.

Unfortunately, many model formulations for vapor compression cycles demonstrate significant variations in the total system charge that do not correspond to observed behavior in experimental systems [6]. This is significant because the dynamics associated with variations in the cycle charge will be coupled to the other system dynamics and introduce aberrant behavior that would not be observed in an experimental system. The dynamics of the refrigerant mass may also be important of themselves, particularly as pertains to ongoing efforts to develop cycles with minimized refrigerant charge [7]. Finally, the relative ease and precision with which the refrigerant mass can be measured can be invaluable in calibrating dynamic models of these systems to experimental data.

One contribution to the related field of evaporator charge management was documented in [6], in which the authors develop a moving-boundary formulation of a single evaporator that conserves refrigerant mass. Other previous work related to the dynamics associated with the cycle charge includes [4], in which the authors study the effect of system oscillations and numerical instability resulting from variations in the density in an evaporator, as well as the work of [25], which discusses both chattering (oscillations around a phase boundary) and the selection of different state variables due to different parameterizations for the equations of state for various fluids.

This paper explores and identifies the causes of these variations in the cycle charge, and develops an alternative modeling approach using a different choice of state variables that successfully conserves refrigerant mass. As will be discussed in the following sections of the paper, these mass variations are caused by interactions between the numerical behavior of the DAE solver and the thermodynamic properties of the refrigerant in the neighborhood of the saturated liquid line for the conventional choice of pressure and specific enthalpy as state variables. The success of an alternative modeling methodology on cycles using the refrigerant R410a is demonstrated using dynamic models of both a simplified refrigerant loop and a full cycle model. Both of these models were developed in the Modelica language. The model of the simplified refrigerant loop is used to eliminate extraneous complexity and demonstrate the salient characteristics of the models that cause variations in the cycle charge, while the full model is used to illustrate the benefits of the alternative approach on a realistic high-order system model similar those used in industry.

One additional effect that is significant for experimental systems, but which has been neglected for this initial study, is that of the interactions between the refrigerant and oil contained in the system. While some of the refrigerant charge in

experimental systems is dissolved in the oil and a charge inventory that ignores this effect will inevitably be lower than an experimentally observed system charge, the challenges inherent in modeling the refrigerant-oil interactions and the need for initial work in this area prompted a focus on single-component working fluids.

Following this introduction, Section 2 discusses the physical and numerical sources of the variation in the cycle charge in the context of a finite volume pipe model, as well as an alternative approach for state selection that can eliminate these variations. Section 3 discusses the construction and implementation of the conservative and nonconservative component models used in the cycle models, as well as an approach for initializing these models to achieve a specified cycle charge. The results of simulating these modified models to eliminate the fluctuations in cycle charge are then discussed in Section 4 for a simplified refrigerant loop model which is used to focus on the refrigerant flow dynamics, as well as a realistic complete cycle model of an air-source heat pump. The final section summarizes and presents conclusions from the work presented in the paper.

## 2. Cycle Mass Variation

Basic vapor compression cycles consist of a compressor, an expansion valve, and two heat exchangers. Common simulation architectures are designed to take advantage of the different timescales for the dynamics of the different components; since the time constants of the compressor and expansion valve are such smaller than those of the heat exchangers, algebraic models are used for these components, and dynamic models are used for the heat exchangers. One common type of model for the heat exchanger dynamics used in this research are so-called finite volume models, which discretize the partial differential equations (PDEs) describing the mass, momentum, and energy conservation in the system. The resulting model formulation consists of a set of ordinary differential equations (ODEs) that can be integrated forward in time to study the dynamics of the system, as well as a set of algebraic constraints including those introduced by the compressor and expansion valve models. While the high complexity of the finite volume models makes them somewhat slower than other heat exchanger modeling approaches, they are quite popular due to their ability to describe spatial variations in the heat exchanger behavior [9, 11, 15].

As is the case with the development of any physical system model, it is essential to clearly define the purpose for which a model is constructed to ensure that it uses an appropriate set of assumptions to describe the desired behavior. Model assumptions used in this work include that of one-dimensional pipe flow, thermodynamic equilibrium in each discrete volume of the refrigerant pipe at each instant in time, a negligible effect of gravitational forces, and a homogeneous flow field in the two-phase region, meaning that the liquid and vapor velocities are equal. These assumptions were employed to avoid additional complexity in the models in an effort to focus on the underlying causes of variations in the cycle mass.

Under these assumptions, the PDEs describing the conservation equations for a



application of the different indices. In addition, the term  $H_k$  is defined as

$$H_k = \dot{m}_k \bar{h}_{upstream,j}, \quad (7)$$

and the mixed-cup specific enthalpy  $\bar{h}$  is equal to the *in situ* specific enthalpy under the homogeneous flow assumption [15].

Thermodynamic property relations also play an important role which is complementary to that of the differential equations of fluid motion. These algebraic property relations describe the relations between the intensive and extensive properties for a given volume of fluid in thermodynamic equilibrium. These properties include temperature, pressure, specific enthalpy, and density, among many others. As a result of the Gibbs phase rule, there are two degrees of freedom for a single-component pure fluid when there is only one phase present, so that knowledge of two intensive properties is sufficient to determine any other property. When the fluid is in the two-phase region, there is only one degree of freedom, but the specification of an intensive mixture property is also needed to determine the state of the two-phase mixture [3]. For example, the specification of pressure  $P$  and mixture specific enthalpy  $h$  will theoretically allow the calculation of any other properties in the thermodynamic phase space.

The calculation of thermophysical properties for dynamic simulation generally needs to be fast and accurate, due to the number of function evaluations used in a typical system model. As a result, the use of standard equations of state is often discouraged in favor of other interpolating methods, such as cubic polynomials or splines [2]. Such methods use function approximation to describe each of a set of desired properties as a function of a limited set of properties that are calculated at each time step in the simulation. Many thermophysical property routines for refrigerants use  $P$  and  $h$  as coordinates in the function approximation space to quickly calculate the variety of necessary properties.

The construction of a dynamic model of the refrigerant in a pipe must therefore take into consideration both the structure of the equations of fluid motion and the implementation of the thermophysical property calculation methods to generate a computationally efficient simulation. The selection of the wrong set of coordinates in which to integrate the conservation equations (4)–(6) can result in the generation of a large set of nonlinear equations that must be solved to calculate the fluid properties at every time step and for every fluid volume, resulting in both numerical and practical challenges. Consequently, it is often essential that the differential equations of fluid motion be implemented in the same coordinates as are used to calculate the refrigerant properties.

The most common approach taken in this regard is the selection of pressure  $P$  and specific enthalpy  $h$  as the state variables for the equations of motion, since these are often also used as the coordinates for calculating the fluid properties. Using this

parameterization, the derivatives of  $M(P, h)$  and  $U(P, h)$  can be written as

$$\frac{dM}{dt} = V \left( \frac{d\rho(P, h)}{dt} \right) \quad (8)$$

$$= V \left( \left. \frac{\partial \rho}{\partial P} \right|_h \frac{dP}{dt} + \left. \frac{\partial \rho}{\partial h} \right|_p \frac{dh}{dt} \right) \quad (9)$$

$$\frac{dU}{dt} = V \left( \frac{d(\rho(P, h)u(P, h))}{dt} \right) \quad (10)$$

$$= V \left[ \left( h \left. \frac{\partial \rho}{\partial P} \right|_h - 1 \right) \frac{dP}{dt} + \left( \left. \frac{\partial \rho}{\partial h} \right|_p h + \rho \right) \frac{dh}{dt} \right]. \quad (11)$$

The use of these property relations, along with the `stateSelect` attribute, can help a Modelica tool to select  $P$  and  $h$  as the state variables for the model. By selecting these properties as state variables, they can be integrated by the solver used in a given Modelica tool, such as DASSL or Radau IIa. Other symbolic and numerical computation techniques, such as event detection and discontinuity handling, are also necessary to ensure the proper behavior of the simulation due to nonlinear and discontinuous behavior of the resulting set of simulation equations.

Many variables in these dynamic models can be affected by the selection of thermodynamic coordinates used to integrate the differential equations. One particular variable that is strongly affected by the choice of state variables is the total mass of the system  $M_{total}$ . Since no mass is stored in the compressor or expansion valve models, an expression for  $M_{total}$  can be developed by summing all of the masses for the individual control volumes in the pipe models, e.g.,

$$M_{total} = \sum_j \rho_j V_j = \sum_j \rho_j(P, h) V_j. \quad (12)$$

Because the integration of the state variables results in some error, however, it is important to note that a more accurate description of this sum might be

$$M_{total} = \sum_j \rho_j(P + \epsilon_1, h + \epsilon_2) V_j, \quad (13)$$

where  $\epsilon_i$  is related to the error tolerance of the integration routine. While these integration errors are not problematic in many fluid regions for which the relation between  $P$ ,  $h$ , and  $\rho$  is nearly linear, two-phase refrigerant flows experience large changes in density as the fluid passes from the liquid region into the two-phase region. These large changes in density can be seen in Figure 2; at the static quality of zero for the given pressure, it is evident that there is a discontinuous change in the derivative of density with respect to the static quality, and hence with respect to the mixture specific enthalpy. Integration errors that are added to state variables located barely on the single-phase side of the saturated liquid line can therefore cause the resulting refrigerant density to be calculated on the two-phase side of that saturation line. Such errors in these density calculations will result in changes to the refrigerant mass in a given control volume and thereby affect the system mass inventory. Moreover, the strong coupling between the refrigerant mass and other system variables, such as pressures and specific enthalpies, will cause local

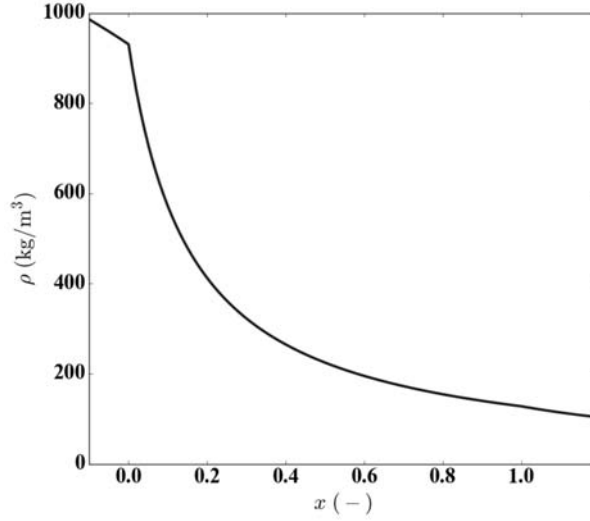


Figure 2. Refrigerant density of R410a as the static quality varies from a subcooled liquid to a superheated vapor at a pressure of 2850 kPa.

disturbances to the refrigerant state to quickly propagate throughout the system. Small integration errors can thus accumulate quickly and lead to significant and unexpected changes in the total system mass.

A comparison of the partial derivatives of the density on either side of the saturated liquid line illustrates the fact that this discontinuity is related to the fundamental thermodynamic characteristics of the fluid. These relations can generally be deduced from Bridgman's table [3]; considering first the properties of the single-phase fluid, the partial derivative of density with respect to pressure and specific enthalpy are

$$\left. \frac{\partial \rho}{\partial h} \right|_P = \frac{\left. \frac{\partial \rho}{\partial T} \right|_P}{\left. \frac{\partial h}{\partial T} \right|_P} = -\frac{\beta \rho}{c_p} \quad (14)$$

$$\left. \frac{\partial \rho}{\partial P} \right|_h = \frac{-T\beta^2 + \beta + \kappa \rho c_p}{c_p}, \quad (15)$$

where  $\beta$  is the isobaric coefficient of expansion,  $\kappa$  is the isothermal compressibility, and  $c_p$  is the specific heat capacity at constant pressure. Each of these properties can be calculated from the state variables through a fundamental equation of state [21].

The partial derivatives of the density with respect to pressure and specific enthalpy in the two-phase region can be calculated similarly [24]. For ease of computation, it is often useful to compute the derivatives of pressure and specific enthalpy not with respect to density, but rather with respect to specific volume; these two sets of derivatives can be interrelated through the identity

$$\frac{\partial \nu}{\partial \rho} = -\frac{1}{\rho^2}. \quad (16)$$

The homogeneous model of two-phase fluid flow can be used to express the mixture specific volume as

$$\nu = \hat{x}\nu_g + (1 - \hat{x})\nu_f, \quad (17)$$

where the static quality  $\hat{x}$  [15] is equal to

$$\hat{x} = \frac{h - h_f}{h_g - h_f}. \quad (18)$$

This can be used to derive an expression for the partial derivative of specific volume with respect to specific enthalpy, e.g.,

$$\left. \frac{\partial \nu}{\partial h} \right|_P = \frac{\nu_g - \nu_f}{h_g - h_f}. \quad (19)$$

The partial derivative of specific volume with respect to pressure can similarly be written as

$$\left. \frac{\partial \nu}{\partial P} \right|_h = \frac{d\nu_f}{dP} + \frac{d\hat{x}}{dP}(\nu_g - \nu_f) + \hat{x} \left( \frac{d\nu_g}{dP} - \frac{d\nu_f}{dP} \right), \quad (20)$$

where the derivatives of density at the saturated liquid and vapor lines are

$$\frac{d\nu_f}{dP} = \beta_f \nu_f \frac{dT}{dP} - \kappa_f \nu_f \quad (21)$$

$$\frac{d\nu_g}{dP} = \beta_g \nu_g \frac{dT}{dP} - \kappa_g \nu_g, \quad (22)$$

the derivative of static quality with respect to pressure is

$$\frac{d\hat{x}}{dP} = \frac{\hat{x} \frac{dh_g}{dP} + (1 - \hat{x}) \frac{dh_f}{dP}}{h_g - h_f}, \quad (23)$$

and the derivatives of specific enthalpy for each phase along the saturation lines are

$$\frac{dh_f}{dP} = \nu_f(1 - \beta_f T) + c_{p,f} \frac{dT}{dP} \quad (24)$$

$$\frac{dh_g}{dP} = \nu_g(1 - \beta_g T) + c_{p,g} \frac{dT}{dP}. \quad (25)$$

Finally, the derivative of temperature with respect to pressure can be derived from the Clapeyron equation,

$$\frac{dT}{dP} = T \frac{\nu_g - \nu_f}{h_g - h_f}. \quad (26)$$

A comparison of the single-phase derivatives listed in Equations (14) and (15) to the two-phase derivatives listed in Equations 19 and 20 demonstrates that these

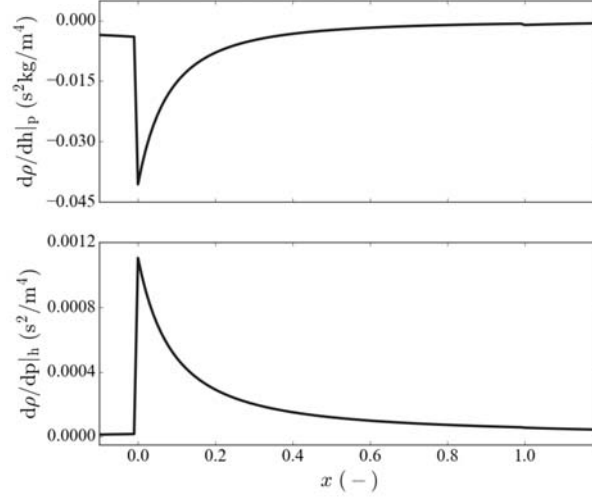


Figure 3. Density derivatives across the saturated liquid line at a pressure of 2850 kPa.

derivatives are not equivalent across the phase boundary. Beyond purely theoretical considerations, this can also be seen in Figure 3, which illustrates the partial derivatives of density with respect to pressure and specific enthalpy for the implementation of the properties of R410a found in the AirConditioning/ThermoFluidPro library [19] for the Modelica tool Dymola [8]. A sharp discontinuity is visible in both of these derivatives at a static quality of zero, again suggesting that errors in the state variables that occur during integration of the differential equations which result in the calculation of the density on the other side of the saturated liquid line will lead to changes in the system mass inventory.

Further consideration of Equation (12) suggests an alternative choice of state variables that can reduce these undesirable changes in the refrigerant mass; since the ultimate objective of reducing nonphysical variations in the system charge is equivalent to reducing the errors in the cell density calculations, the selection of  $\rho$  as a state variable will allow the integrator to minimize the errors in the density directly, rather than through  $\rho(P, h)$ . By choosing  $P$  and  $\rho$  as state variables, the amplification of the errors observed in the density will be eliminated, resulting in a corresponding reduction in the variation of the total system mass.

This alternative selection of state variables results in the following expressions for the derivatives of  $M(P, \rho)$  and  $U(P, \rho)$  for each control volume, e.g.,

$$\frac{dM}{dt} = V \frac{d\rho}{dt} \quad (27)$$

$$\frac{dU}{dt} = \frac{d(\rho u(P, \rho)V)}{dt} \quad (28)$$

$$= V \left[ \left( \rho \frac{\partial h}{\partial P} \Big|_{\rho} - 1 \right) \frac{dP}{dt} + \left( \frac{\partial h}{\partial \rho} \Big|_P + h \right) \frac{d\rho}{dt} \right]. \quad (29)$$

The selection of  $\rho$  does impose additional costs upon the simulation. Perhaps the most significant of these is that the use of  $\rho$  as a state variable will cause the solver to take smaller time steps because of these large values of the derivatives. In addition, this selection of state variables will also affect the final set of equations

that are generated because the change in coordinates will result in the construction of a different set of equations to calculate the remaining fluid properties, e.g., the calculation of  $h(P, \rho)$ . In the case that these equations are nonlinear, the simulation time could also be longer than would be for the case with the selection of the original state variables. However, these costs may be outweighed by the benefit of having a constant cycle charge.

Another alternative method for describing the dynamics of the differential control volume involves expanding the number of state variables to include pressure, specific enthalpy, and density. While this approach does result in a larger number of state variables, it has the advantage of simultaneously minimizing the variations in system charge while enabling the use of  $P$  and  $h$  for calculating other refrigerant properties. Because  $P$  and  $h$  are used as state variables, a smaller set of nonlinear equations will be generated as compared to models that solely use  $P$  and  $\rho$  as state variables. This will result in an improvement in the simulation time over the  $(P, \rho)$  simulations. Such a method uses the same differential equations as the  $(P, \rho)$  model, but also includes the additional ODE

$$\frac{dh}{dt} = \frac{\partial h}{\partial P} \Big|_{\rho} \frac{dP}{dt} + \frac{\partial h}{\partial \rho} \Big|_P \frac{d\rho}{dt}. \quad (30)$$

While this approach in theory relaxes the constraint forcing the state variable being integrated  $h$  to be equal to the computation of the specific enthalpy as a function of the other state variables, e.g.,  $\hat{h}(P, \rho)$ , simulations presented later in the paper provide evidence that these deviations are small in practice.

The set of property derivatives  $\partial h/\partial P$  and  $\partial h/\partial \rho$  from Equations (27) and (29) do not need to be separately calculated in the property routine to use  $P$  and  $\rho$  as state variables. The original set of property derivatives can instead be manipulated to provide the needed derivatives, i.e.,

$$\frac{\partial h}{\partial P} \Big|_{\rho} = - \frac{\partial \rho}{\partial P} \Big|_h \frac{\partial h}{\partial \rho} \Big|_P \quad (31)$$

$$\frac{\partial h}{\partial \rho} \Big|_P = \frac{1}{\frac{\partial \rho}{\partial h} \Big|_P}. \quad (32)$$

### 3. Mass Conserving Cycle Models

Two cycle models, described in the following section, were created to evaluate the efficacy of these alternative state variable selection methods at maintaining constant refrigerant mass in the cycle. A simplified refrigerant loop model was initially developed to facilitate the study of the pipe dynamics without extraneous system complexity; this cycle model included only a refrigerant pipe and the necessary components to enforce the mass and energy balances for the conservation equations. These state selection methods were also subsequently tested on a dynamic model of an complete air-source heat pump to evaluate their practical application. Details about the components for both of these cycle models will be discussed in the following subsections, as well as the means of initializing the simplified cycle to achieve a specified system charge.

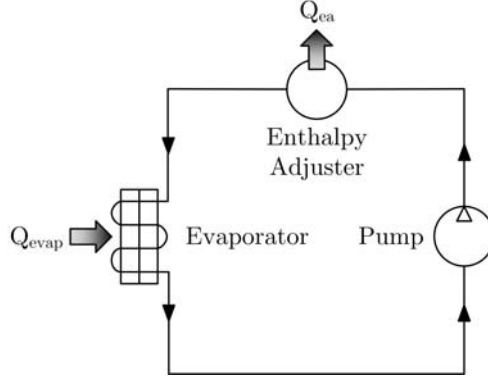


Figure 4. Simplified cycle model to test mass dynamics for closed cycle.

### 3.1. Component Models: Simplified Loop

The simplified cycle model developed in this section, illustrated in Figure 4, includes a refrigerant pipe and two additional components to maintain the mass and energy balances in the cycle: a pump and an “enthalpy adjuster”. While the main focus of this work is the refrigerant pipe, a pump is also needed to enforce mass conservation in the system and define a relation between the mass flow rate and the pressure drop across the pipe, so that these variables can be controlled and modified to examine their effect on the total cycle mass. An additional component, referred to as an enthalpy adjuster, was also used to enforce the conservation of energy throughout the system; this component included no pressure drop, but only modified the enthalpy of the working fluid flowing through it so that energy was conserved over the cycle. Neither the pump nor the enthalpy adjuster stored any refrigerant mass; consequently, these components had no state and imposed only algebraic constraints on the system to achieve a desired system balance point. State variables were therefore only associated with the refrigerant pipe.

A simplified pipe model, governed by the equations described in Section 2, was developed to test the impact of the state variable selection on the dynamics of the cycle charge. In addition to the governing ODEs, these models also required the inclusion of a set of closure relations describing the heat transfer and the frictional pressure drop. An ideal heat transfer connection was assumed for the sake of simplicity, so that the thermal energy was directly added to the refrigerant stream in each control volume, rather than being governed by the temperature gradients between the refrigerant pipe wall and the bulk fluid. A simplified relation for the frictional pressure drop in both the single and two-phase regions was also assumed, in which

$$\Delta P = K \frac{(\Delta P)_0}{\dot{m}_0^2} \dot{m}^2, \quad (33)$$

and the nominal values of  $(\Delta P)_0$  and  $\dot{m}_0$  were set at the top level of the model.

One particularly important feature of the pipe model was the ability to use and interchange different models for the relations between the property derivatives. This was achieved by implementing the set of differential models as a replaceable model inside the larger pipe model. Each pipe model includes its own differential volume

model, but computes the same terms  $dMs$  and  $dUs$ . While each of the underlying differential models implements different relationships between the properties, the instantiating pipe model only needs to equate the derivatives of the mass and internal energy to the terms on the right hand side of Equations (4)–(6). This is demonstrated in the following simplified Modelica code excerpt from the refrigerant pipe model.

```
// DIFFERENTIAL VOLUME MODEL
replaceable model DifferentialModel=DifferentialModel_ph
  constrainedby PartialDifferentialModel;

DifferentialModel diffVolume(
  redeclare Medium=Medium,
  n=n,
  fluidVolumes=fluidVolumes,
  ps={mediums[k].p for k in 1:n},
  hs={mediums[k].h for k in 1:n},
  ddhps={mediums[k].ddhp for k in 1:n},
  ddphs={mediums[k].ddph for k in 1:n},
  stateChoice=stateChoice);

equation
  dms = diffVolume.dms;
  dUs = diffVolume.dUs;
```

By further establishing a parent `PartialDifferentialModel` from which all of the child differential models can inherit, volume models can be replaced while maintaining some moderate restrictions on the possible types of replacement. This enables the state variables to be changed without affecting any of the other parts of the pipe model.

The pump model used a scaled version of the basic relationship between mass flow rate and pressure drop (Equation 33) to calculate the pressure rise across the pump for the nominal pump speed that is inversely proportional to the pressure drop for pipe model including a given number of control volumes, e.g.,

$$\dot{m} = \left( \frac{N}{N_{nom}} \right)^2 \frac{\dot{m}_0 \sqrt{(\Delta P)_0}}{\sqrt{(\Delta P)}}. \quad (34)$$

This relation is based upon conventional pump affinity laws [1] and is valid under the assumption that the flow/pressure drop relation for the load also has a quadratic characteristic. As no mass was stored in this component, the mass flow rates into and out of the pump were equal, and the energy change across the pump was a quadratic function that compensated for the change in enthalpy across the pipe due to pressure loss. This can be expressed as

$$\dot{m}h_{out} = \dot{m}h_{in} + W_{pump}, \quad (35)$$

where the expression for  $W_{pump}$  was calibrated for the simulation. This term was much smaller than the energy change in the pipe due to the heat flux into the pipe.

An analogous enthalpy adjuster model was also created to compensate for the change in the specific enthalpy across the pipe due to the applied heat flux. This

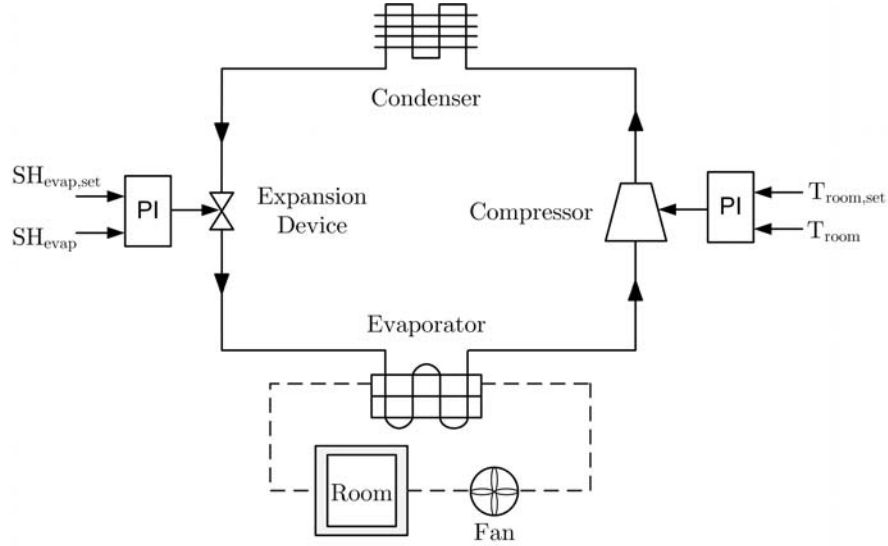


Figure 5. Air-source heat pump cycle model to evaluate mass dynamics for realistic system.

model included no pressure drop or mass storage, and only modified the specific enthalpy for the working fluid flowing out of this component to be equal to the total applied thermal energy gain of the fluid as it traveled through the pipe. This can be expressed as the following conservation equation,

$$\dot{m}h_{out} = \dot{m}h_{in} + Q_{pipe}, \quad (36)$$

where magnitude of  $Q_{pipe}$  is equal to the magnitude of the total amount of thermal energy transferred to the refrigerant pipe and the sign is opposite to maintain the total amount of energy in the system. The stream connector functionality of the Modelica language [10] was also used in these individual components to improve the numerical robustness of the simulation to direction-switching mass flows.

### 3.2. Component Models: Air-Source Heat Pump Cycle

While the simplified loop model provided valuable insights into refrigerant mass dynamics imposed by the structure of the two-phase fluid model, the performance of these different modeling approaches was also evaluated on a full-scale dynamic model of an air-source heat pump operating in cooling mode, such as is illustrated in Figure 5 and described in [14]. Dynamic models were thus developed for a variable speed compressor, an electronically-actuated expansion valve, and a wet-coil heat exchanger, as well as a simplified lumped-parameter model of a room. Because the dynamics of the compressor and expansion valve evolve much faster than the dynamics of the heat exchangers or the room, algebraic models were used for both of these components. These component models were used to construct a model of a complete vapor compression cycle that was calibrated to data collected from an experimental system [15], and thereby evaluate the impact that these changes in state variable selection on the dynamics of the refrigerant mass.

The heat exchanger model was comprised of three main submodels: a model of the

fluid flow on the refrigerant side, a model of the pipe wall, and a model of the air-side fluid flow. Each of these models was composed of an interconnected set of control volume models to account for the spatial variations in the heat exchanger behavior. For example, each refrigerant-side fluid control volume model was connected to a control volume model of the pipe wall and an air-side fluid control volume model. As the heat exchanger was discretized into  $N$  segments, this resulted in  $N$  interconnected refrigerant-side control volumes,  $N$  wall models, and  $N$  interconnected air-side control volumes. These air-side control volumes implemented similar conservation equations as were used on the refrigerant-side, though they were modified to account for the additional assumption of no mass or energy storage in the control volumes due to the low heat capacity and compressibility of the air.

The main structure and frictional pressure drop for the refrigerant-side model of the previous section was employed for this larger model because of its high degree of spatial resolution and its flexibility. The heat transfer calculation for this model was modified by replacing the ideal heat transfer characteristic with a constant phasic heat transfer characteristic; constant values of the heat transfer coefficient, as determined by the flow quality, were used for each phase of the fluid. Numerical instabilities and chattering that could potentially result from discontinuities when transitioning between fluid regions were reduced by using a  $C^2$  continuous smoothing function [23] for values of the flow quality between  $0 \leq x \leq 0.05$  and  $0.95 \leq x \leq 1.0$ . The volumetric flow rate through the air-side of the coils was specified, as well as the inlet air temperature and relative humidity. Additional details relating to these models can be found in [22].

In addition to this refrigerant pipe model, we developed a set of dynamic models of the refrigerant wall that described the wall as one-dimensional heat conduction perpendicular to the fluid flow, and which assumed that there was no axial heat transfer down the pipe. This simple modeling approach employed convective boundary conditions, and is described by the one-node thermal capacitance given by

$$(m_w c_w + m_{fin} c_{fin}) \frac{dT_w}{dt} = \alpha_{ref} A (T_r - T_w) + \dot{m}_{air} [c_{p,air} (T_{air,in} - T_{air,out}) + (\omega_{air,in} - \omega_{air,out}) \Delta h_{fg}]. \quad (37)$$

Similarly, the heat and mass transfer equations on the air side are given by

$$\dot{m}_{air} c_{p,air} \frac{dT_{air}}{dy} \Delta y = \alpha_{air} (A_{o,tube} + \eta_{fin} A_{o,fin}) (T_w - T_{air}) \quad (38)$$

$$\dot{m}_{air} \frac{d\omega_{air}}{dy} \Delta y = \alpha_m (A_{o,tube} + \eta_{fin} A_{o,fin}) \min(0, \omega_{w,sat} - \omega_{air}), \quad (39)$$

where  $\Delta y$  is the discretized length of the tube in the direction of the air flow,  $\omega_{w,sat}$  is the humidity ratio of the air calculated at the wall temperature,  $\eta_{fin}$  is the fin efficiency, and other symbols are given in the nomenclature section in the appendix. The fin efficiency is calculated using the equation proposed by Hong and Webb [12], while the mass transfer coefficient  $\alpha_m$  is calculated via the Lewis analogy

$$\alpha_m = \frac{\alpha_{air}}{c_{p,air} Le^{2/3}} \quad (40)$$

where  $Le^{2/3} = 0.9$  [13].

An isenthalpic model of the expansion valve, with neither mass nor energy storage, was used to describe the expansion process. The mass flow rate through the expansion device is related to the valve orifice size  $\theta$ , the inlet refrigerant density  $\rho_{in}$ , and the pressure drop across the valve  $P_{in} - P_{out}$ , e.g.,

$$\dot{m}_{EEV} = \theta \sqrt{\rho_{in}(P_{in} - P_{out})}. \quad (41)$$

A simple compressor model, also with no mass or energy storage, was also used [13]. This model describes the mass flow rate of refrigerant through the compressor and the change in the specific enthalpy of the refrigerant as it travels from the suction port to the discharge port, e.g.,

$$\dot{m} = \eta_v \rho_{suc} V N \quad (42)$$

$$\eta_v = a_1 \frac{P_{dis}}{P_{suc}} + a_2 \quad (43)$$

$$h_{dis} = h_{suc} + \frac{h_{dis,is} - h_{suc}}{\eta_{is}} \quad (44)$$

$$h_{dis,is} = f(p_{suc}, h_{suc}), \quad (45)$$

where the constants  $a_1$  and  $a_2$ , as well as the maps for the volumetric efficiency  $\eta_v$  and the isentropic efficiency  $\eta_{is}$ , are determined through a compressor performance test and are built from polynomial expansions of the compressor speed and the pressure ratio.

A room model was also required to test the dynamics of the closed-loop heat pump system, since the system cannot be tested under load without a feedback controller to regulate the room air temperature and other salient internal process variables, such as the evaporator superheat. A lumped adiabatic thermal capacitance model was used to describe the room. In this model, the sum of the sensible and latent cooling capacities of the machine were matched to the sensible and latent loads imposed in the room in steady-state, while the controller regulated the transient behavior of the machine to achieve the specified process variable setpoints. In addition, the total mass balance in the room was modified by including the water vapor injected by the latent load as well as the water flow rate out of the room due to dehumidification; this was equal to the latent cooling capacity of the machine divided by the heat of vaporization of the water.

### 3.3. Initialization

The problem of achieving a specified constant charge for a cycle simulation can be effectively split into two related problems: the initialization of the simulation so that the cycle mass starts at the specified value, and the maintenance of the cycle charge at that value over the duration of the simulation. While the previous sections of the paper address how to maintain the cycle charge at a constant value, this brief section addresses the means by which a specific value of the cycle charge may be attained for the simplified loop system. In general, the total refrigerant mass contained in the cycle at initialization depends on the initial refrigerant state in each volume of the system. Because the refrigerant state at zero mass flow rate is relatively easy to determine, the simplified loop system was initialized at this condition so that the pump speed was zero and no heat flux was applied to the pipe

Table 1. Common parameters for the test cycle models.

Pipe diameter	8 mm
Pipe length	12 m
Maximum heat input	130 W/cell (3120 W total)
Initial pressure	1 MPa
Initial system charge	150 g
Number of pipe control volumes	24

or the enthalpy adjuster. These inputs were turned on after the conclusion of the initialization transient.

The initial conditions for the system were developed using basic thermodynamic reasoning. The specification of a value of cycle charge  $M_{total}$  for a given system volume  $V$  effectively specifies the average density of the fluid in the system  $\rho_{init}$ ; this specifies one variable that determines the state of the system. Independent specification of one other variable for the system, such as the system pressure  $P_{init}$  at zero pump speed and zero heat flux, determines the state of the refrigerant in the system. The specific enthalpy  $h_{init}$  for every component and control volume can therefore be directly calculated from this refrigerant state in a set of initial equations. Since it is common to initialize most components with values of pressure and specific enthalpy, these calculated initial values for the working fluid were then used to initialize all of the components in the system to achieve the desired cycle charge.

## 4. Results

The collection of component models described in the previous section was used to create two cycle models to evaluate the effect of these different state variable choices on the mass dynamics of the system. The transient behavior of the simplified loop model is discussed first to illustrate a number of pertinent behaviors of the mass dynamics that are solely associated with the refrigerant fluid model, and then the transient behavior of the air-source heat pump model will be presented to assess the analogous effects on a conventional system architecture.

Both of these system models were implemented in Modelica using the R410a refrigerant model included in the AirConditioning/ThermoFluidPro library, as well as the simple relationship between frictional pressure drop and mass flow rate described in Equation 33, where  $(\Delta P)_0 = 500$  Pa and  $\dot{m}_0 = 10$  g/s. For each system, three related models were created with identical geometric parameters and input waveforms to study the effect of the alternate state variable choices. These models were tested in simulation using Dymola 2015 FD01, and were executed on an i7 PC with 8G of RAM; the DASSL solver was used to integrate all of these models forward in time.

### 4.1. *Simplified Loop Model*

Physics-based models often necessitate the use of a large number of parameters to describe the system construction. Some of the most salient parameters for this first simplified loop model are included in Table 1. Because the variations in the cycle charge are related to phase transitions in the fluid volumes across the saturated liquid line, a series of inputs was designed to repeatedly produce these transitions in an effort to induce variations in the cycle charge. These input waveforms, both

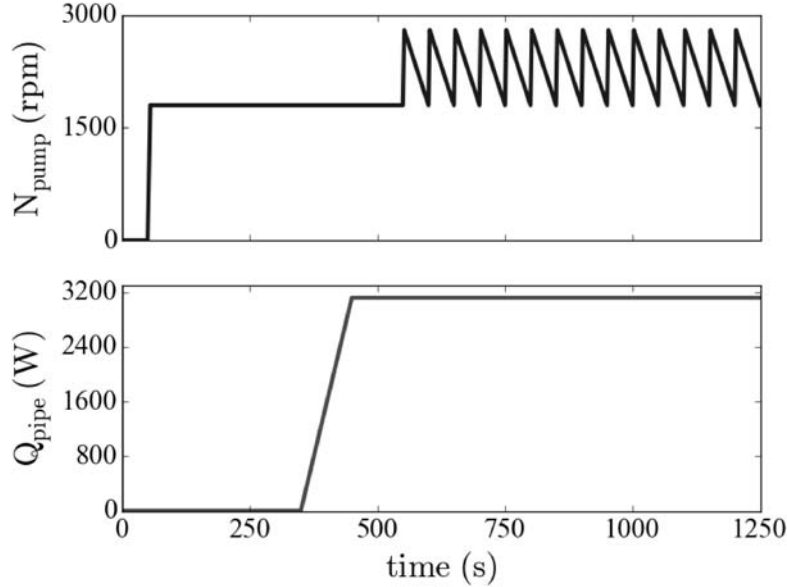


Figure 6. Inputs of pump speed (upper) and heat input (lower) applied to the test cycle.

for the pump speed and the heat source, are illustrated in Figure 6. After the cycle was initialized with the specified refrigerant mass and zero mass flow rate, the pump speed was ramped up at 50 seconds from 0 to 1800 rpm over 5 seconds. The resulting transients were then allowed to subside before ramping up the heat source at  $t = 350$  seconds over 100 seconds from 0 to 3120 W, with the heat being distributed equally over each of the 24 control volumes in the pipe. Finally, a ramp sawtooth waveform was applied to the pump speed to repeatedly cause transitions across the liquid saturation line; the resulting pump speed had a minimum value of 1800 rpm, a maximum value of 2800 rpm, a period of 50 seconds, and a duty ratio of 0.052. All of the simulations used identical input waveforms.

The effect of this waveform on the model using  $P$  and  $h$  as state variables are illustrated in Figure 7. While many notable features are evident, perhaps the most striking aspect is the amount of variability in the total cycle charge. These large changes in the total cycle charge can be quite problematic, as they will have a significant impact on the behavior of the cycle. It is evident that the amount of variation in the total cycle mass is strongly correlated with the tolerance of the solver, suggesting that the variation is indeed related to the integration tolerances. Moreover, the changes in the mass inventory usually occur by steps, suggesting the presence of a discontinuity that gives rise to these changes.

Figure 8 illustrates the relation between the discontinuity caused by the changes in the static quality  $x = M_{\text{vap}}/M_{\text{total}}$  for control volumes 1, 2, and 3 and the variations in the total system charge. The dashed line drawn at  $t = 603$  seconds shows a strong correlation between the time that the static quality for all three of these control volumes goes above zero and the time of the step discontinuity in the total system charge. It is particularly interesting to note that while the quality of the third control volume increases above zero a number of subsequent times in this plot, there are no other variations in the total system charge. This phenomenon suggests that the variations in the refrigerant charge are related not only to a transition

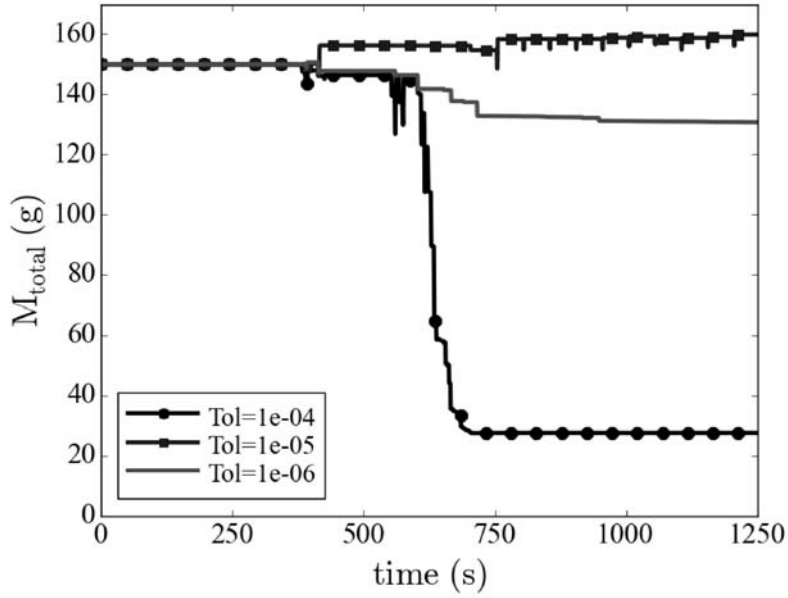


Figure 7. Total cycle mass for three different numerical tolerances with identical applied inputs.

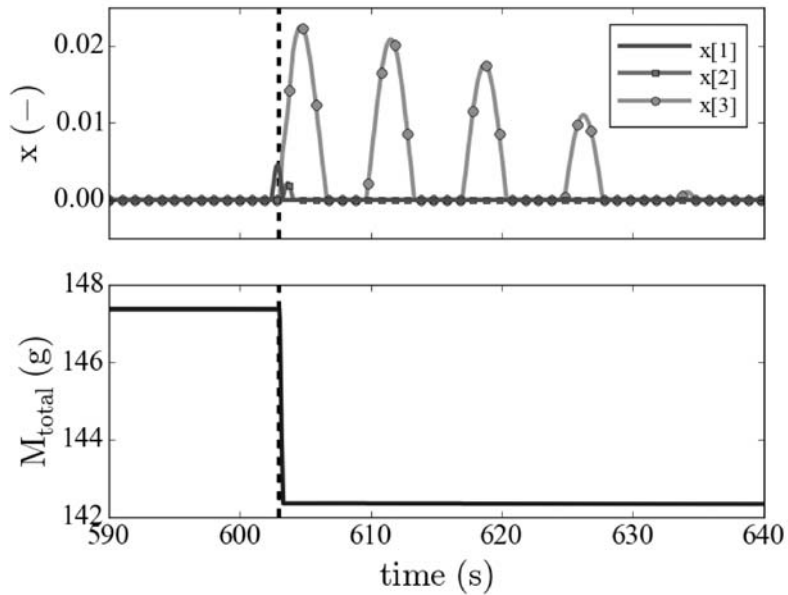


Figure 8. Static quality  $x$  at the first, second, and third control volumes in the pipe with  $(P, h)$  states during the increasing portion of the pump speed waveform, as well as the total system charge at the same moment. A solver tolerance of  $1\text{e-}4$  was used for this simulation.

across the liquid saturation line, but also to the rate and duration of this transition. The small magnitude of the abrupt excursions over  $x = 0$  for control volumes 1 and 2 are associated with large changes in the refrigerant density, as well as with the corresponding large changes in the cycle mass, are compatible with the assertion that the variations in the total system charge could be caused by the errors in the state variables.

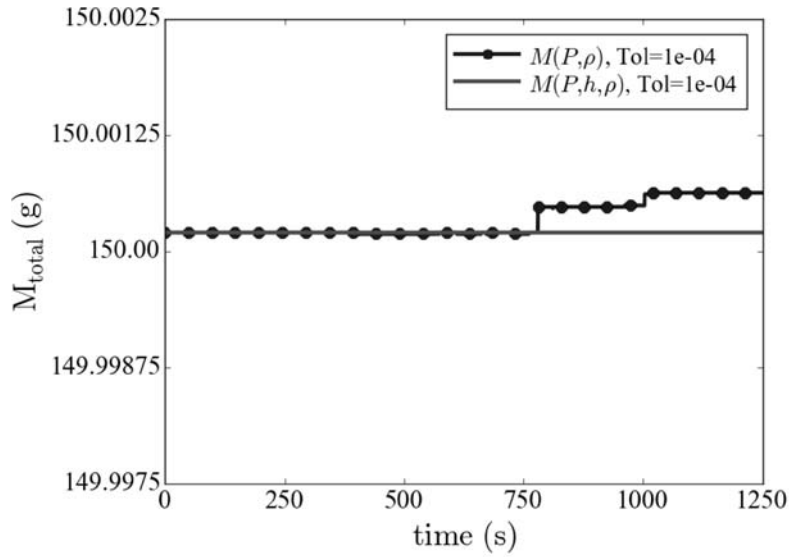


Figure 9. Cycle mass inventory for  $M(P, \rho)$  and  $M(P, h, \rho)$  models, with an integration tolerance of  $1e-04$ .

Table 2. Max and percentage errors and CPU time for different choices of state variables and integrator tolerances.

State Var	Tol	Max Error	% Error	CPU Time
$M(P, h)$	$1e-4$	-122.6 g	81.7%	277 s
	$1e-5$	3.96 g	2.6%	127 s
	$1e-6$	-19.3 g	12.8%	1925 s
$M(P, \rho)$	$1e-4$	$1.9e-4$ g	$1.2e-4\%$	766 s
	$1e-5$	$2.0e-4$ g	$1.3e-4\%$	1250 s
	$1e-6$	$2.0e-4$ g	$1.3e-4\%$	1374 s
$M(P, h, \rho)$	$1e-4$	$2.0e-4$ g	$1.3e-4\%$	137 s
	$1e-5$	$2.0e-4$ g	$1.3e-4\%$	315 s
	$1e-6$	$2.0e-4$ g	$1.3e-4\%$	450 s

In comparison to the large variations in the total system charge exhibited in Figure 7 for the system using  $(P, h)$  as state variables, the minuscule variations present in Figure 9 demonstrate that the models that use either  $(P, \rho)$  and  $(P, h, \rho)$  as state variables have much improved behavior. The variations in the mass for both of these cycles are on the order of 0.25 milligrams, or  $1.7 \times 10^{-4}\%$  of the total cycle charge. This compares quite favorably to the output of the simulation of the  $(P, h)$  model with the same tolerance, which resulted in an 82% change in the total cycle charge. Further reductions in the error tolerance for the  $(P, \rho)$  and  $(P, h, \rho)$  simulations will result in a corresponding reduction in the variation in the total cycle charge.

Additional insights can be gained from the information contained in Table 2, which compares the errors in the simulations and the total time required to run each simulation for different sets of state variables and error tolerances. The errors in this table were generated by calculating the maximum deviation between the total system charge and 150.0 grams, which was the specified charge. As might be expected, the error in the total system charge is far greater for the model with the  $(P, h)$  state variables than for the other models. It is also interesting to note that the simulation time for the  $(P, h)$  model with a tolerance of  $1e-6$  is much greater than for any of the other simulations for any combination of state variables. This can potentially be attributed to the presence of so many discontinuities in the simulation

Table 3. Common parameters for the test cycle models.

Pipe diameter	8 mm
Evaporator pipe length	16 m
Condenser pipe length	16 m
Room sensible heat load	2000 W
Room latent heat load	200 W
Ambient temperature	35 °C
Ambient relative humidity	45 %
Room air temperature setpoint	25 °C
Initial system charge	150 g
Number of evaporator control volumes	24
Number of condenser control volumes	24

waveform due to the changes in the refrigerant mass; since the solver must take very small time steps past each discontinuity to maintain the specified error tolerance, the sum effect of these discontinuities is that the average time step of the solver must be much smaller than might otherwise be necessary.

Comparison of the simulation time of the  $(P, h)$  models to the  $(P, \rho)$  models indicates that the  $(P, \rho)$  models are slower because the large variations in refrigerant density cause the solver to take correspondingly smaller time steps and because of the increased number of nonlinear equation systems that must be solved. It is also evident from Table 2 that the  $(P, \rho)$  and  $(P, h, \rho)$  methods have nearly identical accuracy, but that the time required to run the  $(P, h, \rho)$  simulations is much smaller than that of the  $(P, \rho)$  simulations. This speed-up can be best understood by considering that the  $(P, \rho)$  model has 24 more nonlinear equation blocks (equal to the number of control volumes in the pipe) than both the  $(P, h)$  and the  $(P, h, \rho)$  models; additional time is required to solve this larger set of nonlinear equations.

#### 4.2. Air-Source Heat Pump Model

The parameters of the physical models used to build the air-source heat pump model were chosen to be representative of a machine sized for residential applications. Some of the model parameters, such as the coefficients of the polynomials used to describe  $\eta_v$  and  $\eta_{is}$  were fitted to experimental data. While the sheer number of these parameters precludes their complete inclusion in this paper, particularly relevant parameters for these simulations are listed in Table 3.

Control loops and the adiabatic room model described in Section 3.2 were added to the basic air-source heat pump to evaluate the impact of state variable selection on the mass inventory dynamics of the cycle. These control loops consisted of two decoupled proportional-integral (PI) controllers for regulating the compressor speed and the expansion valve position. The error between the room temperature setpoint and the measured room temperature was input to the PI block controlling the compressor speed, while the error between the evaporator superheat setpoint and the measured evaporator superheat was input to the PI block controlling the expansion valve position. The parameters of these loops were tuned to achieve a relatively fast step response for both of these variables.

As was the case in Section 4.1, three different system models were constructed with the three groups of state variables. Each of these simulations was initialized with same set of pressures and specific enthalpies, resulting in the same initial cycle charge. The same boundary conditions and set of control inputs were also used for each of these models.

Figure 10 illustrates the response of the system to a change in the evaporator

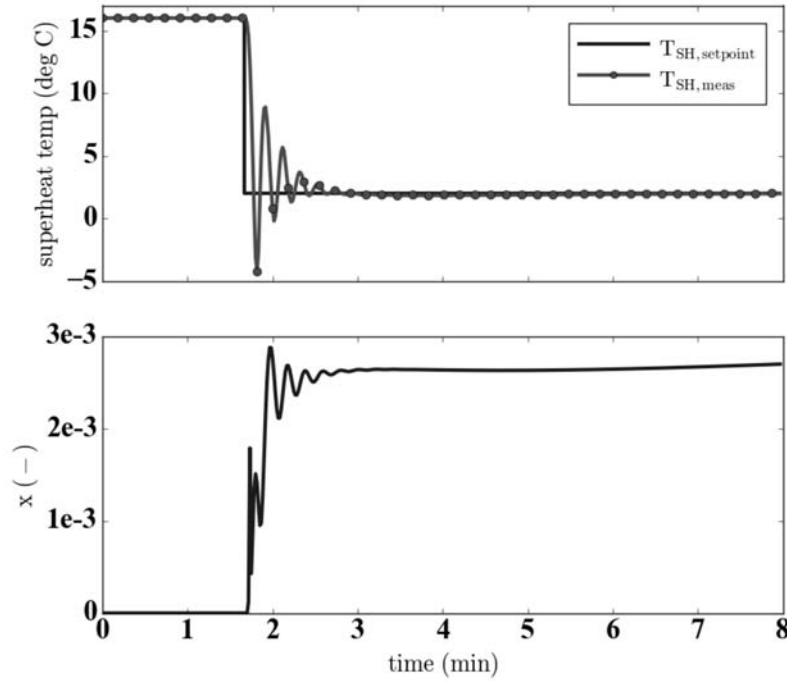


Figure 10. The upper plot illustrates the evaporator superheat setpoint and measurement, while the lower plot illustrates the static quality at the thirteenth control volume in the condenser.

superheat setpoint. In the upper plot of this figure, the step change of the evaporator superheat setpoint from 16 °C to 2 °C can be seen overlaid with the resulting underdamped response of the measured evaporator superheat. This input waveform results in a sudden increase in the quality in the thirteenth control volume of the condenser, due to the sudden change in the condenser pressure, as can be seen in the lower plot of this figure. It is notable that the final quality in this control volume is still quite low, but its rapid movement of the refrigerant state across the saturated liquid line is the feature of note.

As the result of this change in the evaporator superheat setpoint, a significant change is evident in Figure 11 for the model using the  $(P, h)$  state variables. While the simulations with lower solver tolerances are clearly more susceptible to these changes than the simulations with the higher solver tolerances, but it is interesting to note that even the simulation with the solver tolerance of  $10^{-6}$  experiences some variation in the refrigerant charge. As was also the case for the results on the simplified loop model, the correlation between these changes in the mass and the abrupt change in the refrigerant state across the saturated liquid line indicates that the errors in the density derivatives in the neighborhood of this line are responsible for the observed mass dynamics. In the case of simulations that are run on a seasonal or an annual basis, such variations in charge could potentially result in significant deviations in the refrigerant mass over the duration of the simulation. In comparison, the simulations with both the  $(P, \rho)$  and  $(P, h, \rho)$  state variables did not exhibit any significant mass variations: observed changes were on the order of  $10^{-8}$  kg. This data reinforces the results from the previous subsection, suggesting that these state variable choices will be particularly appropriate for dynamic simulations of air-source vapor compression heat pumps where the conservation of refrigerant mass

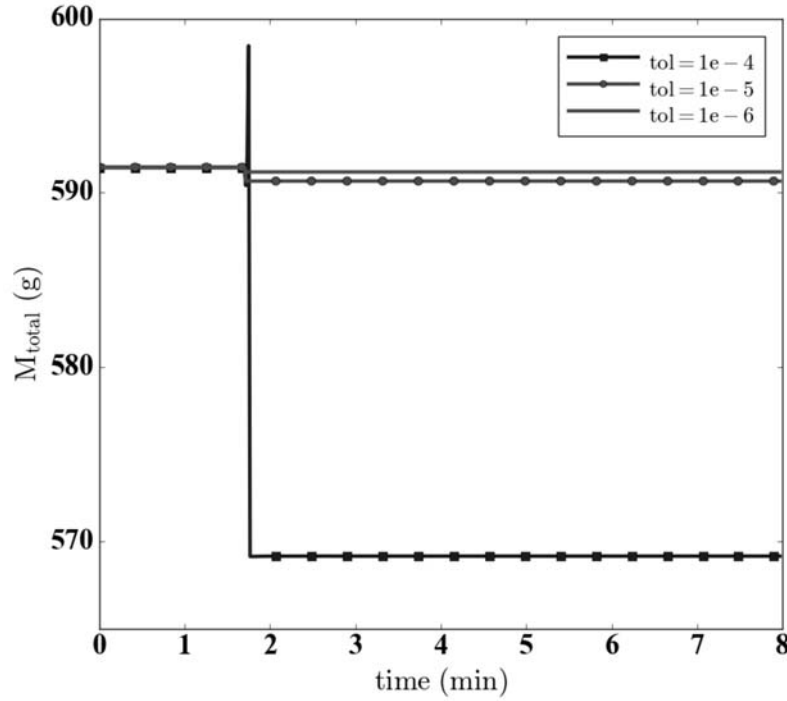


Figure 11. Changes in refrigerant mass for the air-source cycle, showing that the changes to the control variable and the static quality from Figure 10 are highly correlated with the changes in the refrigerant mass.

over long periods of time is important.

Figure 12, which illustrates the CPU time required for the simulation as a function of the time in the simulation, also furnishes further information about the relative merits of each of these state selection approaches. These results are also consistent with those observed in Section 4.1; it is clear that the  $(P, h)$  and the  $(P, h, \rho)$  models both have similar execution time due to the reduced number of nonlinear equations in comparison to the  $(P, \rho)$  model. These nonlinear equations in the  $(P, \rho)$  model cause a notable increase in the simulation time during the step in the evaporator superheat due to the numerical stiffness of the system of equations, which is not seen in the models with other choices of state variables.

The consistency of the thermodynamic parameters for these systems also merits consideration, particularly for the  $(P, h, \rho)$  model, because of the potential for errors between the specific enthalpy calculated from the pressure and density and the specific enthalpy calculated as a separate state variable. Figure 13 illustrates the percentage deviation in the total energy balance for the system for these three models; these deviations were calculated by computing the difference between the total energy contained in the system from the integral form of the energy equation provided in Equation 46 and the total energy contained in the system by summing the internal energies calculated from the state variables, e.g.,

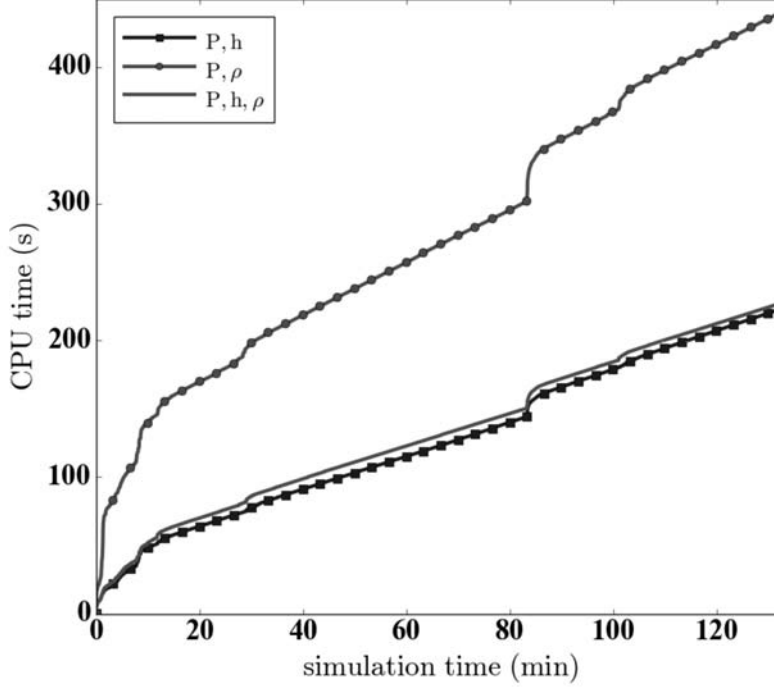


Figure 12. CPU time for cycle simulations for a solver tolerance of  $1e-5$ .

$$U_{true} = \sum_i \int (\dot{m}_{i,in} h_{i,in} - \dot{m}_{i,out} h_{i,out} + \Delta q_i) dt \quad (46)$$

$$\%U_{tot,err} = \frac{\sum_i \rho_i V_i u_i(\xi) - U_{true}}{U_{true}} \times 100, \quad (47)$$

where  $\xi$  represents the choice of the state variables for the system models,  $\Delta q_i$  is the heat transfer rate transferred to or from each control volume, and the sum is taken over all of the control volumes in the model. It is evident from this figure that while the deviations for  $(P, h, \rho)$  model is somewhat higher than those of the  $(P, h)$  model, as expected, the magnitude of these differences are very small. Moreover, it is also notable that the deviation for the  $(P, \rho)$  model are higher than those of the  $(P, h, \rho)$  model; these deviations are likely caused by the challenges associated with solving the increased number of nonlinear equation blocks. The inclusion of the additional state variable in the  $(P, h, \rho)$  model thus appears to improve the simulation speed and mass conservation in the cycle while maintaining acceptable deviations in the system energy balance.

## 5. Conclusions

Over the course of this paper, the causes of variations in the total system charge were studied and two alternative selections of the state variables that can essentially eliminate such variations were proposed. The effect of these different state variable

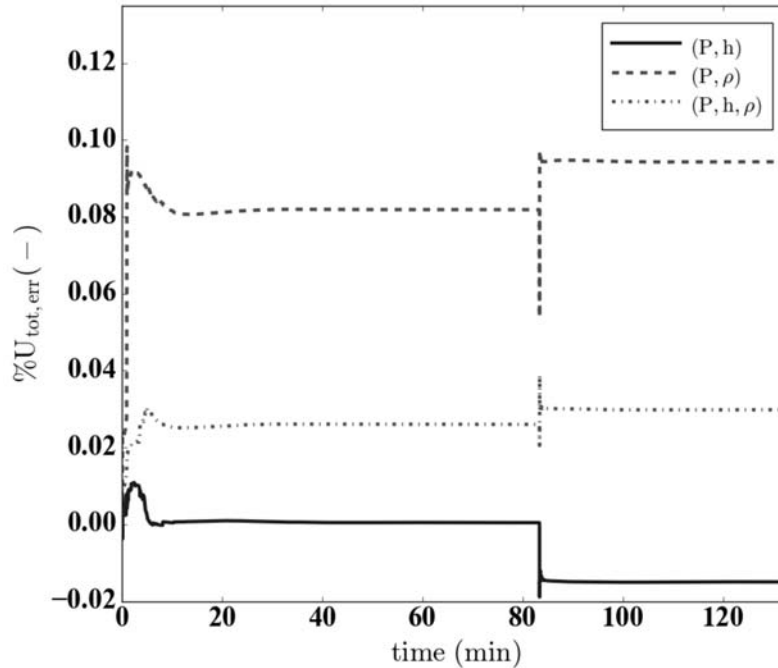


Figure 13. The percentage of error for the total internal energy, defined by Equation (47), for the three different choices of state variables with a solver tolerance of  $1e-5$ .

selections were demonstrated on both a simplified cycle model and a realistic air-source heat pump model, and the manifestations of the underlying causes for the cycle variation when  $P$  and  $h$  are solely used as state variables were examined by analyzing the simulation output. While both the  $(P, \rho)$  and  $(P, h, \rho)$  models had similar accuracy for simulating the total system charge, the  $(P, h, \rho)$  models simulated much faster because  $h(P, \rho)$  does not have to be calculated when it is also included as a state variable. Moreover, though one ostensible motivation for using  $(P, h)$  as state variables is the speed by which the property calculations can be executed, the dynamics associated with the variation in total system charge can somewhat ironically result in simulations that take longer to run than simulations with  $(P, \rho)$  as state variables because of the small step sizes required, as seen in the data illustrated in Table 2. Models for refrigerant pipes that include either  $(P, \rho)$  or  $(P, h, \rho)$  as state variables can therefore result in simulations that are both faster and more accurate than might be possible with a choice of  $(P, h)$  as state variables, though the additional nonlinear equations created when using the  $(P, \rho)$  models often makes them somewhat slower than the other models in practice.

## Nomenclature

## References

- [1] American Society of Heating, Refrigerating, and Air-Conditioning Engineers. *ASHRAE Handbook: HVAC Systems and Equipment*. ASHRAE, 2008.
- [2] V. Aute and R. Radermacher. Standardized polynomials for fast evaluation of refrig-

$A$	cross-sectional area
$F_f$	frictional pressure drop
$M$	mass
$N$	pump speed
$P$	pressure
$Q$	heat transfer rate
$U$	internal energy
$T$	temperature
$V$	volume
$W$	compressor work
$a_i$	polynomial coefficients
$c_p$	specific heat capacity at constant pressure
$h$	<i>in situ</i> specific enthalpy
$\bar{h}$	“mixed-cup” specific enthalpy
$l$	control volume length
Le	Lewis number
$\dot{m}$	mass flow rate
$q$	heat flow input
$t$	time
$u$	specific internal energy
$v$	velocity
$x$	flow quality
$\hat{x}$	static quality
$\alpha$	heat transfer coefficient
$\beta$	isobaric coefficient of expansion
$\theta$	expansion valve orifice size
$\kappa$	isothermal compressibility
$\nu$	specific volume
$\rho$	density
$\omega$	humidity ratio
$f$	liquid, speed
$g$	gas
<i>cond</i>	condenser
<i>dis</i>	compressor discharge port
<i>evap</i>	evaporator
<i>suc</i>	compressor suction port
<i>is</i>	isentropic

erant thermophysical properties. In *International Refrigeration and Air-Conditioning Conference at Purdue*, 2014.

- [3] A. Bejan. *Advanced Engineering Thermodynamics*. Wiley, 3 edition, 2006.
- [4] J. Bonilla, L.J. Yebra, and S. Dormido. Chattering in dynamic mathematical two-phase flow models. *Applied Mathematical Modeling*, 36:2067–2081, 2012.
- [5] G.E.P. Box and N.R. Draper. *Empirical Model-Building and Response Surfaces*. Wiley, 1987.
- [6] L. Cecchinato and F. Mancini. An intrinsically mass conservative switched evaporator model adopting the moving-boundary method. *International Journal of Refrigeration*, 35:349–364, 2012.
- [7] J.M. Corberan, I. Martinez-Galvan, S. Martinez-Ballester, J. Gonzalez-Macia, and R. Royo-Pastor. Influence of the source and sink temperatures on the optimal refriger-

- ant charge of a water-to-water heat pump. *International Journal of Refrigeration*, 34: 881–892, 2011.
- [8] AB Dassault Systemes. Dymola, 2014.
  - [9] H. Elmqvist, H. Tummescheit, and M. Otter. Object-oriented modeling of thermo-fluid systems. In *Proceedings of the 3rd Modelica Conference*, 2003.
  - [10] R. Franke, F. Casella, M. Otter, M. Sielemann, H. Elmqvist, S-E. Mattson, and H. Olsson. Stream connectors: An extension of Modelica for device-oriented modeling of convective transport phenomena. In *Proceedings of the 7th Modelica Conference*, 2009.
  - [11] R. Franke, F. Casella, M. Sielemann, K. Proelss, M. Otter, and M. Wetter. Standardization of thermo-fluid modeling in Modelica.Fluid. In *Proceedings of the 7th Modelica Conference*, 2009.
  - [12] K.T. Hong and R.L. Webb. Calculation of fin efficiency for wet and dry fins. *HVAC&R Research*, 2(1):27–41, 1996.
  - [13] T.H. Kuehn, J.W. Ramsey, and J.L. Threlkeld. *Thermal Environmental Engineering*. Prentice Hall, 3 edition, 1998.
  - [14] C. Laughman. A comparison of transient heat pump cycle simulations with homogeneous and heterogeneous flow models. In *International Refrigeration and Air Conditioning Conference at Purdue University*, 2014.
  - [15] C. Laughman, H. Qiao, V. Aute, and R. Radermacher. A comparison of transient heat pump cycle models using alternative flow descriptions. *Science and Technology for the Built Environment*, 21(5):666–680, 2015.
  - [16] P. Li, Y. Li, J.E. Seem, H. Qiao, X. Li, and J. Winkler. Recent advances in dynamic modeling of HVAC equipment. Part 2: Modelica-based modeling. *HVAC&R Research*, 20(1):150–161, 2014.
  - [17] P. Li, H. Qiao, Y. Li, J.E. Seem, J. Winkler, and X. Li. Recent advances in dynamic modeling of HVAC equipment. Part 1: Equipment modeling. *HVAC&R Research*, 20(1):136–149, 2014.
  - [18] Modelica Association. Modelica specification, version 3.3, 2014. URL [www.modelica.org](http://www.modelica.org).
  - [19] Modelon AB. *Air Conditioning Library User Guide*, 2015. v1.9.0.
  - [20] S.V. Patankar. *Numerical Heat Transfer and Fluid Flow*. Hemisphere Publishing Co., 1980.
  - [21] H. Qiao. *Transient Modeling of Two-Stage and Variable Refrigerant Flow Vapor Compression Systems with Frosting and Defrosting*. PhD thesis, University of Maryland, 2014.
  - [22] H. Qiao, V. Aute, and R. Radermacher. Transient modeling of a flash tank vapor injection heat pump system - part i: Model development. *International Journal of Refrigeration*, 2014.
  - [23] C.C. Richter. *Proposal of New Object-Oriented Equation-Based Model Libraries for Thermodynamic Systems*. PhD thesis, Technical University of Braunschweig, 2008.
  - [24] M. Thorade and A. Saadat. Partial derivatives of thermodynamic state properties for dynamic simulation. *Environmental Earth Sciences*, 70(8):3497–3503, 2013. .
  - [25] H. Tummescheit. *Design and Implementation of Object-Oriented Model Libraries using Modelica*. PhD thesis, Lund Institute of Technology, 2002.